Engineering Science and Technology, an International Journal 23 (2020) 240–252

HOSTED BY

Contents lists available at ScienceDirect

Engineering Science and Technology, an International Journal

journal homepage: www.elsevier.com/locate/jestch

# Coordinated tuning of controller-parameters using symbiotic organisms search algorithm for frequency regulation of multi-area wind integrated power system

Sugandh P. Singh [a], Tapan Prakash [b,*], Vinay Pratap Singh [b]

[a] Department of Electrical Engineering, Indian Institute of Technology Kanpur, Kanpur 208016, India
[b] Department of Electrical Engineering, National Institute of Technology Raipur, Raipur 492010, India

ARTICLE INFO

*Article history:*
Received 9 August 2018
Revised 13 February 2019
Accepted 19 March 2019
Available online 3 May 2019

*Keywords:*
Automatic generation control
Doubly-fed induction generator
Multi-area power system
Proportional-integral-derivative controller
Symbiotic organisms search algorithm

ABSTRACT

Presently, the integration of renewable energy into existing power system to cater increasing power needs is a growing trend. Wind energy is one of the prominent utilized renewable sources. However, the generation level of integrated wind energy significantly affects the frequency characteristics of entire system. Further, if the control scheme of wind systems are not properly working then this situation may deteriorate the frequency characteristics of whole system. Therefore, it is indispensable to tune the parameters of controllers of existing and wind systems in proper coordination so as to improve the frequency characteristics of the system. Consequently, in this work, a coordinated tuning of parameters of controllers to improve frequency characteristics of a multi-area interconnected thermal system in presence of doubly-fed induction generator (DFIG) based wind generation is presented. A widely used two-area non-reheat thermal interconnected system is simulated having its one area integrated with DFIG based wind generation. The parameters of controllers of thermal and wind systems are coordinately tuned using symbiotic organisms search (SOS) algorithm. Different design objectives are framed to achieve improved frequency characteristics of entire system. The considered objectives are combined together by proper assignment of weights using analytic hierarchy process to form a single objective function. Several test cases with diverse disturbances under different wind penetration levels are conducted to test the performance of system with SOS based controllers. To further assess the effectiveness of proposed controllers, other controllers using differential evolution (DE), elephant herding optimization (EHO), particle swarm optimization (PSO) and teaching-learning-based optimization (TLBO) are also designed and comparatively tested under the considered cases.


## 1. Introduction

To cater the needs of growing power demand and to maintain generation and load equilibrium, electric utilities are opting for interconnections of existing networks and integration of renewable energy into the system. Though these developments may fulfill the power demand but at the same time they may affect the secure and reliable operation of entire system. Furthermore, load demand is highly unpredictable and therefore, it becomes difficult to maintain generation and load equilibrium [1]. If there is any mismatch between generation and load and if it stays for long time then this may affect the system frequency and voltage profile. In general, active power balance (APB) is responsible for keeping system nominal frequency (SNF) and reactive power balance keeps flat voltage profile of the system. APB can be achieved by a control mechanism termed as automatic generation control (AGC) [2]. Thus, the prime contribution of AGC is to keep system frequency and power through tie-line within allowable limits in case of occurrence of any disturbance in the system.

Presently, integration of renewable energy into existing system is a fast growing trend. These integrations offer several advantages but at the same time may affect the functioning of existing system. Out of several renewable energy sources, wind energy achieved through wind energy conversion system (WECS) is one of the preferred choices. However, the concerns towards increasing levels of wind penetration and their impact on the existing system is continuously raisng. It is found that the wind generation levels significantly affect the frequency regulation characteristics (FRC) of the system [3]. Therefore, it in indispensable to study the role of wind

* Corresponding author.
*E-mail address:* tapanprakashsinha@gmail.com (T. Prakash).

https://doi.org/10.1016/j.jestch.2019.03.007
2215-0986/

**Nomenclature**

*Acronyms*

| | |
|---|---|
| ABC | Artificial bee colony |
| ACE | Area control error |
| AGC | Automatic generation control |
| AHP | Analytic hierarchy process |
| APB | Active power balance |
| DE | Differential evolution |
| DFIG | Doubly fed induction generator |
| EHO | Elephant herding optimization |
| FA | Firefly algorithm |
| FD | Frequency deviation |
| FR | Frequency regulation |
| FRC | Frequency regulation characteristic |
| GA | Genetic algorithm |
| GM | Geometric mean |
| IPS | Interconnected power system |
| ITAE | Integral of time multiplied absolute error |
| JA | Jaya algorithm |
| MOP | Multi-objective problem |
| NSCS | Non-dominated sorting cuckoo search |
| NSGA-II | Non-dominated sorting genetic algorithm-II |
| PD | Proportional-derivative |
| PI | Proportional-integral |
| PID | Proportional-integral-derivative |
| PO | Peak overshoot |
| PSO | Particle swarm optimization |
| RES | Renewable energy source |
| SLP | Step load perturbation |
| SNF | System nominal frequency |
| SOS | Symbiotic organism search |
| ST | Settling time |
| TDS | Time-domain simulation |
| TLBO | Teaching-learning based optimization |
| TLPD | Tie-line power deviation |
| VSWT | Variable speed wind turbine |
| WECS | Wind energy conversion system |
| WITS | Wind integrated thermal system |
| WPG | Wind power generation |

*List of symbols*

| | |
|---|---|
| $M_V$ | Mutual vector |
| $1, 2$ | Subscripts representing Area 1 and Area 2, respectively |
| $\alpha_1, \alpha_2$ | Random numbers in the range 0 and 1 |
| $\beta$ | Factor in the range [−1,1] |
| $\Delta f$ | Frequency deviation |
| $\Delta f_{11}$ | Permanent frequency deviation |
| $\Delta f'_{11}$ | Stabilized frequency deviation output |
| $\Delta P_{12}$ | Net change in power exchange between two areas in p.u. |
| $\Delta P_d$ | Load demand perturbations |
| $\Delta P_G$ | Change in governor valve position in p.u. |
| $\Delta P_{tie}$ | Tie-line power deviation |
| $\Delta P_T$ | Change in output power of turbine in p.u. |
| $\mu$ | Scale factor |
| $\omega$ | Scale factor |
| $\omega_i$ | Relative weights ($i = 1, 2, 3.$) |
| $a_{12}$ | Constant equal to $-1$ |
| $B$ | Frequency bias factor |
| $c_1$ | Cognitive parameter |
| $c_2$ | Social parameter |
| $C_R$ | Crossover rate |
| $F_1$ | First design objective |
| $F_2$ | Second design objective |
| $F_3$ | Third design objective |
| $H$ | Inertia constant |
| *Iter_MAX* | Maximum iteration |
| $K_D$ | Derivative gain |
| $K_I$ | Integral gain |
| $K_P$ | Proportional gain |
| $K_{Df}$ | Proportional gain of PD controller |
| $K_{Pf}$ | Derivative gain of PD controller |
| $K_{PS}$ | Power system gain |
| $M$ | Pair-wise comparison matrix |
| $M_F$ | Mutation factor |
| $m_{ij}$ | $i$th row and $j$th column element of the matrix $M$ |
| $n$ | Derivative term of filter |
| *norm* | Superscript for normalized value |
| $P_f^*$ | Reference power output |
| $P_V$ | Parasite vector |
| *PIDn* | PID controller with derivative filter |
| *po* | Superscript representing peak-overshoot |
| $R$ | Governor speed regulation constant |
| $S_D$ | Size of each organisms i.e. number of decision variables |
| $S_{POP}$ | Population size |
| *st* | Superscript representing settling time |
| $T_G$ | Governor time constant |
| $T_s$ | Simulation time |
| $T_T$ | Time constant of turbines in seconds |
| $T_{PS}$ | Time constant for power system in seconds |
| $TF_{PIDn}$ | Transfer function of *PIDn* controller |
| $u$ | Controller output |
| $w$ | Inertia weight |
| $W_{PL}$ | Wind penetration level |
| $X$ | Solution vector |
| $X_p$ | $p$th organism ($p = 1, 2, \ldots, S_{POP}$) |
| $X_p^{new}$ | $p$th new solution |
| $X_q$ | $q$th solution |
| $X_q^{new}$ | $q$th new solution |
| $X_{best}$ | Best organism |
| $K_{Wp}, K_{Wi}$ | Design parameters of PI controller of DFIG |
| min, max | Superscripts used for minimum and maximum, respectively |

energy and the impact of wind generation levels on regulating frequency of the system. Out of several WECS, doubly-fed induction generator (DFIG) driven by variable speed wind turbines (VSWTs) are more preferred due to presence of power electronics interface and pitch angle control. It is known that the response of WECS towards frequency regulation is quite different from thermal generators [4]. If any requirement of regulating system frequency by maintaining APB arises, then the stored kinetic energy in DFIG driven by VSWTs is utilized to provide temporary active power support [5,6].

It is reported in literature that large penetration of wind power generation (WPG) using DFIG into conventional system reduces overall inertial response potential of system [7–9]. However, restoration of inertial response of system is possible with introduction of appropriate supplementary control structure in DFIG [7,8,10–12]. In [7], modifications in DFIG control system is carried out to establish inertial response to DFIG wind turbines. A field controlled DFIG considering generator model of fifth-order is explained in [8]. The work reported in [10] suggests the necessity of changes in reserve policies or certain modifications in wind tur-

bine inertial response characteristics in order to counter frequency excursions. A control strategy providing DFIG with ability to regulate frequency on short term basis is investigated in [11]. In [12], a method is presented which enables VSWT to emulate inertia resulting in providing support to primary frequency control. Further, the work reported in [13] draws attention towards an approach, to provide support to SNF, derived on the basis of inertial control taking account of faster response of WECS. In this approach, the rotational masses of WECS storing kinetic energy is used to support the frequency excursions. In [14], an analysis is performed on the active participation of DFIG to responses of the SNF of a multi-area interconnected power system (IPS). Similar work is carried out in [15] showing the performance of DFIG in frequency regulation (FR) mode or maximum power tracking mode depending upon frequency requirements or system conditions.

An efficient controller for DFIG is primarily required to achieve better FR. The design of controllers for DFIG should be performed in coordination to the controllers of AGC so that there are no adverse effects onto the performance of controllers of AGC. The conventional proportional-integral-derivative (PID) controller [16,17] is preferred controller structure due to its simplicity and easy implementation [18]. In case of controllers of DFIG, a proportional-derivative (PD) and a proportional-integral (PI) controllers are used for inertial control. However, the proper coordinated tuning of AGC and DFIG controllers is an important aspect in achieving better performance. Various methods based on optimization algorithms are reported in literature to perform tuning of parameters of controllers for AGC of a multi-area IPS. Some relevant algorithms used for tuning controller-parameters are particle swarm optimization (PSO) [19,20], non-dominated sorting genetic algorithm-II (NSGA-II) [21], differential evolution (DE) [22], artificial bee colony (ABC) algorithm [23], teaching-learning based optimization (TLBO) [24], firefly algorithm (FA) [25], and Jaya algorithm (JA) [18]. The application of intelligent techniques to perform optimal power flow (OPF) of WITS is more attended area of research [26–29] while the task of coordinated tuning of controllers for improving FRC for WITS based on intelligent techniques is reported in limited numbers like PSO [30,31], genetic algorithm (GA) [32], NSGA-II [33], non-dominated sorting cuckoo search (NSCS) algorithm [34], etc. This motivated the present work to carry coordinated tuning of controllers for FR of a WITS.

Apart from the tuning algorithms, appropriate selection of design objectives is required to tune parameters of controllers properly in order to attain satisfactory performance. For an AGC problem, the design objectives can be the minimization of time-domain specifications like settling times (STs) and peak overshoots (POs) of FDs and tie-line power deviations (TLPDs), integral errors, and/or maximization of damping ratios [21]. The formulated objective function with two or more design objectives produces multi-objective problem (MOP). For some MOP, it is strenuous task to obtain true Pareto-optimal front [35]. The best way to avoid this difficult situation is to form a single objective function by appropriately assigning relative weights to different objectives encountered in MOP.

In this work, a maiden approach based on symbiotic organism search (SOS) algorithm is attempted for coordinated tuning of parameters of controllers for improving FR of wind integrated multi-area IPS. A linearized model of two-area IPS with one area integrated with DFIG farm is examined. The design objectives taken in account are the minimization of the STs of the FDs of the areas with TLPD, minimization of the integral errors and minimization of the POs of FDs and TLPD. This MOP is transformed into a single objective formulation by utilizing analytic hierarchy process (AHP) with appropriate assignment of weights to different objectives. The performance of SOS based controller in improving FR of the system is investigated under diverse sets of wind penetration levels and load disturbances. A comparative assessment of SOS based controller is accomplished by comparing it with other controllers based on PSO, TLBO, DE and elephant herding optimization (EHO). Further, time-domain simulations (TDS) are presented to illustrate the effective performance of the proposed controller. The key contributions of this work are highlighted as:

- FRC of a wind-integrated thermal system with different wind penetration levels is investigated.
- Coordinated tuning of parameters of controllers based on SOS algorithm is presented.
- MOP of minimization is converted into single objective formulation by allocating proper weights to considered objectives encountered in MOP.
- AHP is utilized for obtaining proper weights of different objectives.
- Several case studies of diverse load disturbances in both areas with different wind penetration level are conducted to examine the performance of controller.
- To assess the effectiveness of proposed controller, other controllers using PSO, ABC, TLBO, DE and EHO are also designed and comparisons are carried out.

## 2. System under study

### 2.1. Two area system model with DFIG based WPG

The two-area linearized model of IPS having area 1 equipped with DFIG based WPG is illustrated in Fig. 1. The thermal power generation model studied in this work is non-reheat type. The thermal system model and the parameters used in the model [36] are listed in Appendix A. Controller structure for DFIG based power generation model and its values are taken from [33] and are listed in Appendix B. In Fig. 1, the area control errors (ACEs) of the two areas are denoted by $ACE_1$ and $ACE_2$; the governor speed regulation constants are shown by $R_1$ and $R_2$; $B_1$ and $B_2$ represent frequency bias factors; $u_1$ and $u_2$ are controller outputs serving as control inputs to the speed governing system; governor time constants in seconds are represented by $T_{G1}$ and $T_{G2}$ whereas changes in governor valve positions in p.u. are shown by $\Delta P_{G1}$ and $\Delta P_{G2}$; $T_{T1}$ and $T_{T2}$ are time constants of turbines in seconds, and $\Delta P_{T1}$ and $\Delta P_{T2}$ are changes in output powers of turbines in p. u. The power system gains are represented by $K_{PS1}$ and $K_{PS2}$ whereas the time constants in seconds are shown by $T_{PS2}$ and $T_{PS2}$. $\Delta P_{d1}$ and $\Delta P_{d2}$ represent load demand perturbations. $\Delta P_{tie}$ is TLPD in p.u. whereas $\Delta P_{12}$ is the net change in power exchange between the two areas in p.u. and $a_{12}$ is a constant equal to $-1$. $\Delta f_1$ and $\Delta f_2$ denote FDs of two areas in Hz.

Each area depicted in Fig. 1 possesses its own generator, turbine and speed governing system. DFIG based WPG is added to area 1 only. The ACEs ($ACE_1$ and $ACE_2$) and the FDs ($\Delta f_1$ and $\Delta f_2$) of the two areas are outputs of system. The control inputs ($u_1$ and $u_2$) along with the load demand perturbations ($\Delta P_{d1}$ and $\Delta P_{d2}$) and TLPD ($\Delta P_{tie}$) serve as inputs to system. The controller used in each area is PID controller with derivative filter that is represented in Fig. 1 as *PIDn* controller. The derivative filter reduces noise in input signal. A block diagram representation of *PIDn* controller is shown in Fig. 2. In Fig. 2, $K_P, K_I, K_D$, and $n$ are proportional gain, integral gain, derivative gain and derivative term of filter, respectively. The input to this controller is the ACE ($ACE_1$ or $ACE_2$) of the respective area and output is the control input ($u_1$ or $u_2$) to the governing system of the respective area. The ACEs of the two areas are expressed as:

$$ACE_1 = B_1 \cdot \Delta f_1 + \Delta P_{tie} \tag{1}$$

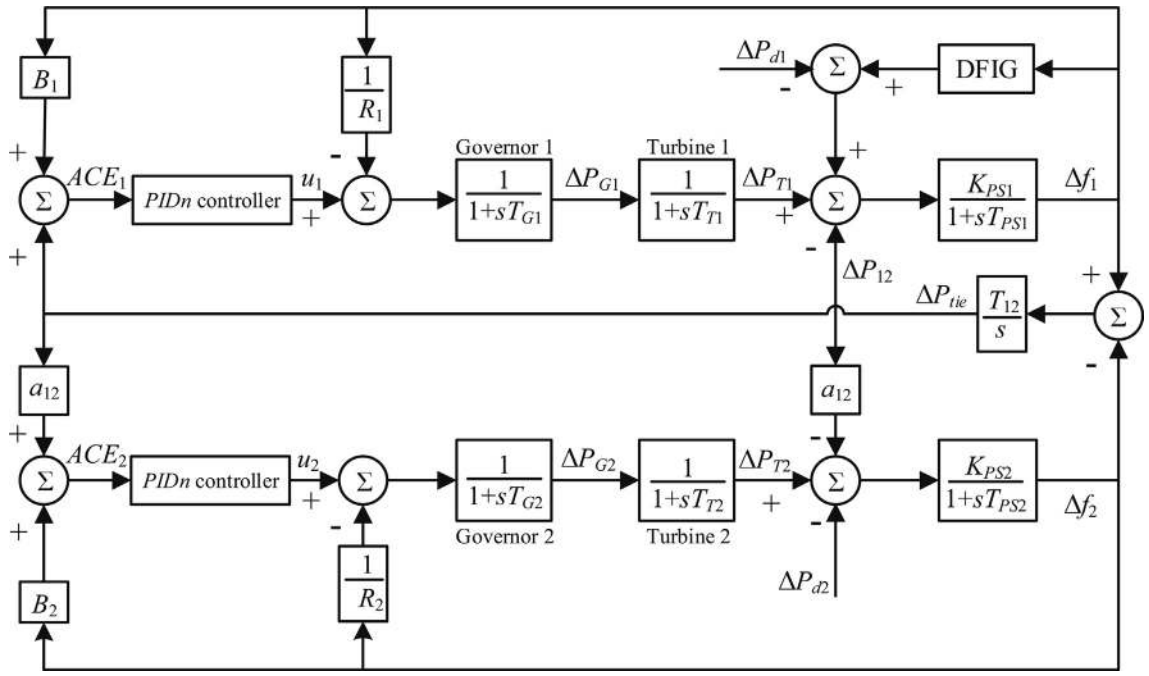


**Fig. 1.** Block diagram of two-area IPS with DFIG.

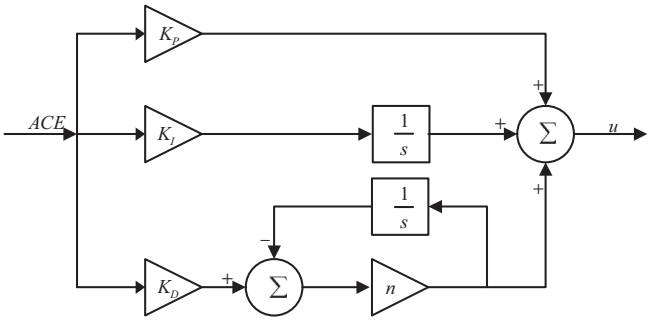


**Fig. 2.** Structure of *PIDn* controller.

$$ACE_2 = B_2 \cdot \Delta f_2 + a_{12} \cdot \Delta P_{tie} \tag{2}$$

The overall transfer function of *PIDn* controller is denoted as

$$TF_{PIDn} = K_P + K_I\left(\frac{1}{s}\right) + K_D s\left(\frac{n}{s+n}\right) \tag{3}$$

### 2.2. DFIG controller

The primary frequency control implemented through AGC compensates the disparity in active power demand and generation in a multi-area IPS. For a wind integrated system, DFIG participation in overall active power generation is fixed as it is always designed to extract maximum power from wind energy. However, DFIG can provide frequency support to system unlike conventional generators. The stored kinetic energy of WECS can be used for primary control of frequency by selecting proper control schemes. Different control schemes for DFIG based WPG are available in literature. A review on these control schemes can be found in [37]. Basically, these control schemes are categorized as inertial control scheme, pitch control scheme, and speed control by de-loaded power extraction curve. In this work, inertial control scheme for DFIG based WPG is focussed. This control scheme essentially contains PD controller, PI controller and washout block. Fig. 3 illustrates the block diagram having inertial control [33]. Brief discussions of the major blocks of the control scheme are as follows:

#### 2.2.1. PD controller

When a DFIG driven by VSWT is integrated with the grid, the contribution of the rotational kinetic energy of DFIG to the inertia of the grid is not inherent due to decoupling of rotational speed from system frequency by grid side converter. However, an arrangement of auxiliary signal for the inertial control scheme can be employed so as to make DFIG based WPG capable of contributing to the inertia of the grid and generating excess active power for frequency support. This arrangement is illustrated in Fig. 3 in which the auxiliary signal adds to the reference power output, $P_f^*$, which is under continuous track of controller of non-conventional generator [12,38,39]. The reference power output, $P_f^*$, is expressed as

$$P_f^* = -K_{Df} \cdot \frac{d\Delta f'_{11}}{dt} - K_{Pf} \cdot \Delta f'_{11} \tag{4}$$

where $K_{Pf}$ is the proportionality constant of the frequency deviation while $K_{Df}$ is the proportionality constant for derivative of frequency deviation. The action undertaken by PD controller to control the transient variations in primary frequency is represented through (4). Whenever the SF crosses certain set limit, it is added into the torque expression to set the torque demand resulting in activating the PD controller. With any increase in load, there is drop in SF which results into the increment of set torque. This phenomenon eventually slows down the rotor speed and the stored kinetic energy is extricated.

#### 2.2.2. PI controller

PI controller helps in retaining the optimal speed of the non-conventional generator of WECS after the end of the transient period. It is required to suitably choose the design parameters ($K_{Wp}$ and $K_{Wi}$) of PI controller in order to have optimal performance characterized by faster recovery of speed with shorter time frame of transient speed alterations [13]. The reduction in speed for

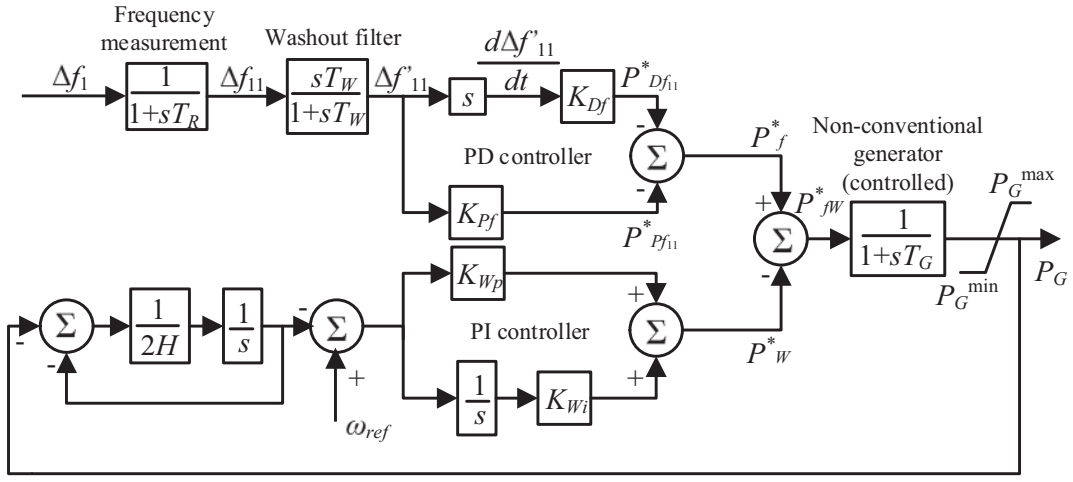


**Fig. 3.** Inertial control scheme of DFIG.

longer duration in due course of improving FR of the system is not allowable as it may lead to stalling of the machine. In this case, the FR is improved by damping of load and by the effects of speed-droop characteristics of the generators.

*2.2.3. Washout filter*

A washout block is used in inertial control scheme as depicted in Fig. 3. It is utilized to restrict the exploitation of DFIG for longer duration while regulating the SF. Non-conventional generators are supposed to extract stored kinetic energy to enhance FR of system only during the transient period and as a result, they cannot sustain a permanent frequency excursion. The washout filter is responsible for stabilizing the permanent FD (i.e. $\Delta f_{11}$) and results in a stabilized FD output $\Delta f'_{11}$. This implies that the permanent frequency deviations do not adversely affect the control scheme.

The active power control capacity of DFIG has the capability of improving FR of system. This implies that inertial contribution from DFIG based generation can be properly adjusted by changing the power setting beyond steady state limit for a given step perturbation $\Delta P_d$ at certain wind penetration level $W_{PL}$. The adjusted power setting can be given as input to the grid side controller of DFIG to extricate the rotational energy from rotor turbine blades [14]. The numerical value of inertia constant, $H$, and regulation droop, $R$, of a WITS changes with change in wind penetration level, $W_{PL}$ [14]. Table 1 shows the values of $H$ and $R$ for different wind penetration levels, $W_{PL}$.

## 3. Problem formulation

In multi-area IPS, the controller performance is influenced by the choice of a design objective. The consideration of single design objective is not sufficient enough to achieve better controller performance. Owing to it, different design objectives are considered together to improve controller performance. This converts design problem into MOP. However, the multi-objective design criterion increases the complexity of the problem and sometimes it is difficult to obtain true Pareto-optimal fronts [35]. A simple method to overcome this difficulty is to change MOP into single objective by allocating appropriate weights to considered design objectives. In this work, three different objectives are considered based on minimization of STs of FDs and TLPD, integral errors, and POs of FDs and TLPD. AHP is utilized to allocate proper weights to the considered objectives in order to formulate a single design objective. In the following sub-sections, different objectives under consideration and single objective design problem formulation by applying AHP are discussed.

**Table 1**
Values of $H$ and $R$ with variation in $W_{PL}$.

| | | Frequency support | | No frequency support | |
|---|---|---|---|---|---|
| $W_{PL}$ | 0% | 10% | 20% | 10% | 20% |
| $H$ | 5 | 4.86 | 4.71 | 4.5 | 4 |
| $R$ | 2.4 | 2.66 | 3 | 2.66 | 3 |

*3.1. Design objectives under consideration*

The first design objective $F_1$ considered in this work is the sum total of STs of the FDs of two areas and TLPD. Whenever the system disturbances or load changes occur, this design objective maintains the power exchange between the areas as soon as possible after such occurrence [1,2]. This design objective is represented as:

$$F_1 = \Delta f_1^{st} + \Delta f_2^{st} + \Delta P_{tie}^{st} \tag{5}$$

where $\Delta f_1^{st}$ and $\Delta f_2^{st}$ are the STs of FDs of control area 1 and area 2, respectively. $\Delta P_{tie}^{st}$ is the ST of TLPD.

The second design objective $F_2$ used in this work is the integral of time multiplied absolute errors (ITAE) of the FDs of the control areas and TLPD. This design objective takes care of setting the frequency and TLPD to zero under sudden load change or disturbance by minimization of the considered integral error [1,2]. It is expressed as:

$$F_2 = \int_0^{T_s} (|\Delta f_1| + |\Delta f_2| + |\Delta P_{tie}|) \cdot t \cdot dt \tag{6}$$

where $T_s$ is simulation time.

The third design objective $F_3$ evaluated in this work is the sum total of POs of the frequencies and TLPD. This design objective is accountable for increasing damping factor which eventually provide adequate degree of stability to the system [1,2]. It is mathematically depicted as:

$$F_3 = \Delta f_1^{po} + \Delta f_2^{po} + \Delta P_{tie}^{po} \tag{7}$$

where $\Delta f_1^{po}$ and $\Delta f_2^{po}$ are the POs of FDs of control area 1 and area 2, respectively. $\Delta P_{tie}^{po}$ is PO of TLPD.

The three design objectives represented in (5)–(7) are integrated together to form a single objective formulation $F$ with appropriate assignment of weights using AHP. However, the three different design objectives $F_1, F_2$ and $F_3$ are normalized using Min-Max normalization method. The formulated objective function is represented as:

$$F = \omega_1 F_1^{norm} + \omega_2 F_2^{norm} + \omega_3 F_3^{norm} \tag{8}$$

where $\omega_1, \omega_2$ and $\omega_3$ are the relative weights assigned to the normalized values $F_1^{norm}, F_2^{norm}$ and $F_3^{norm}$ of design objectives $F_1, F_2$ and $F_3$, respectively.

### 3.2. Implementation of AHP to the problem

AHP is a decision making analytic technique based on defragmenting a problem into a set of hierarchies of the objectives [40,41]. The first step is to assign relative importance to different objectives. In this work, the design objective $F_1$ is considered to be immensely important in comparison to design objectives $F_2$ and $F_3$. The objective $F_1$ given in (5) represents different STs of FDs and TLPD. The settling down of FDs of the control areas and TLPD to zero as soon as possible after the occurrence of any severe load change or disturbance is of prime importance. That is why $F_1$ is considered as most important. The design objectives $F_2$ and $F_3$, given in (6) and (7), respectively, are assigned lower importance as compared to $F_1$.

The next step in AHP is the formation of a pair-wise comparison matrix. The design objective $F_1$ is given the highest importance by assigning a value of 9 and the design objectives $F_2$ and $F_3$ are given lesser importance by assigning values of 7 and 5, respectively. It should be noted that the diagonal entries of comparison matrix will have a numerical value of 1 as it signifies the comparison of the respective design objective with itself. The other entries of the matrix show the relative importance of a design objective to others. The pair-wise comparison matrix $M$ formed after considering above numerical values assigned to different objectives is as follows:

$$M = \begin{bmatrix} 1 & 7 & 9 \\ \frac{1}{7} & 1 & 5 \\ \frac{1}{9} & \frac{1}{5} & 1 \end{bmatrix} \tag{9}$$

After formation of the matrix, the third step of AHP involves the calculation of relative normalized weights $\omega_i (i = 1, 2, 3)$ of each of the three design objectives based on finding the geometric means (GMs) of the $i$th row and normalizing them. The mathematical expression for finding out the GM and its normalization is:

$$\omega_i = \frac{P_i}{\sum_{i=1}^{3} P_i} \tag{10}$$

where $P_i = \left(\prod_{j=1}^{3} m_{ij}\right)^{\frac{1}{3}}$ which is the GM of $i$th row, and $m_{ij}$ is the element of the matrix $M$ for $i$th row and $j$th column.

The relative weights $\omega_1, \omega_2$ and $\omega_3$ calculated using (10) for (9) are $\omega_1 = 0.772, \omega_2 = 0.1734$, and $\omega_3 = 0.0545$. The single objective function $F$ used in this whole work is formed by replacing the values of $\omega_i (i = 1, 2, 3)$ in (8). The final form of objective function becomes

$$F = 0.772 F_1^{norm} + 0.1734 F_2^{norm} + 0.0545 F_3^{norm} \tag{11}$$

The objective function, (11), is minimized using SOS algorithm. Following section describes basic structure of SOS algorithm.

## 4. Symbiotic organisms search (SOS) algorithm

### 4.1. Brief description of SOS algorithm

SOS algorithm is a swarm-based optimization technique reproducing relationship of the organisms living together in an ecosystem [42]. The symbiotic relations among organisms of different species can be beneficial for both species without doing harm to any of them, or can be beneficial for one of the species with other remained unbenefited and unharmed, or can be beneficial for one of the species with other remained unbenefited and harmed. Based on these symbiotic relations, SOS algorithm is classified into three phases: mutualism, commensalism, and parasitism. In this algorithm, ecosystem consisting of organisms of different species is analogous to the population where each organism is representing a candidate solution and the size of organism represents dimension of the problem.

Let us consider that there are $S_{POP}$ organisms of different species in the ecosystem i.e. population size and $S_D$ is the size of each organism i.e. decision variables. $X_p$ represents the $p$th organism $(p = 1, 2, \ldots, S_{POP})$ and the best organism is represented by $X_{best}$.

The interaction characteristic of organisms of different species in an ecosystem defines the basic principle of the phases mentioned above. In mutualism phase, symbiotic interactions benefit both organisms. One organism gets benefited while other remains unaffected in commensalism phase. In parasitic phase, one organism is benefited while other is harmed. The three phases of the algorithm are described below in detail.

#### 4.1.1. Mutualism phase

In this phase, the interactions among organisms provide benefits to both sides without doing harm to anyone. An organism (selected randomly) $X_q$ interacts with organism $X_p$ of the ecosystem to develop a mutual relationship aiming at increasing the chances of survival. New candidate solutions, $X_p^{new}$ and $X_q^{new}$ for $X_p$ and $X_q$, respectively, are obtained according to:

$$X_p^{new} = X_p + \alpha_1 (X_{best} - M_V \times B_{F1}) \tag{12}$$

$$X_q^{new} = X_q + \alpha_2 (X_{best} - M_V \times B_{F2}) \tag{13}$$

where $M_V$ is the mutual vector obtained by $\left(\frac{X_p + X_q}{2}\right)$. The parameters $\alpha_1, \alpha_2 \in [0, 1]$ and $B_{F1}, B_{F2} \in \{1, 2\}$ . The better candidate solutions are accepted. The solution vector $X$ thus obtained takes part in the next phase.

#### 4.1.2. Commensalism phase

In this phase, the interactions among organisms provide benefits to one side while other side remains unbenefited and unharmed. In the same manner to the previous phase, $X_q$ is selected randomly from the ecosystem to interact with $X_p$. However, in this phase, $X_q$ does not get modified as it remains unbenefited and unharmed with the interaction. The new candidate solution $X_p^{new}$ is obtained as:

$$X_p^{new} = X_p + \beta \times (X_{best} - X_q) \tag{14}$$

where $\beta \in [-1, 1]$. The better candidate solutions are accepted. Thus, the obtained solution vector $X$ will take part in the next phase.

#### 4.1.3. Parasitism phase

In this phase, the interactions among the organisms benefit one side while harming the other side. A parasite vector $P_V$ is created after duplicating $X_p$, and, then modified by randomly selecting dimensions. $X_q$ is selected from the ecosystem on random basis serving as the host to $P_V$. Parasite vector $P_V$ replaces $X_q$ in the ecosystem if it found better otherwise $X_q$ is retained in the ecosys-

tem. The new obtained solution vector $X$ after this phase takes part in the next generation. This process is repeated until any stopping criterion is met. The psuedocode of SOS algorithm is presented in Algorithm 1.

**Algorithm 1** Pseudocode of SOS algorithm

```
Ecosystem initialization: Set initial population size S_POP and dimension of the problem S_D.
Define maximum iteration Iter_MAX and boundary conditions for decision variables.
Initialize random population within search space.
for i = 1 : Iter_MAX do
  Evaluate fitness function.
  Identify best solution X_best.
  Mutualism phase starts...
  for p = 1 : S_POP do
    Select a random solution X_q where q ≠ p.
    Obtain vector M_V and factors B_F1 and B_F2.
    Update solution X_p using (12) and X_q using (13).
    Evaluate fitness function and select better solution.
  Mutualism phase ends.
  Commensalism phase starts...
  for p = 1 : S_POP do
    Select a random solution X_q where q ≠ p.
    Update solution X_p using (14).
    Evaluate fitness function and select better solution.
  Commensalism phase ends.
  Parasitism phase starts...
  for p = 1 : S_POP do
    Create a parasite vector P_V from X_q.
    Replace X_q by P_V if P_V has better fitness value.
  Parasitism phase ends.
Final solution.
```

### 4.2. Implementation of SOS algorithm to the problem

For the objective function $F$ stated in (11), six design variables are chosen. Four design variables are the parameters of *PIDn* controllers $(K_P, K_I, K_D, n)$ and used as main controller in both areas while two design variables are parameters of DFIG controller $(K_{Pf}$ and $K_{Df})$ used in area 1. The two parameters of PD controller of DFIG is chosen as design variables based on the sensitivity analysis done in [33]. The sensitivity analysis revealed that parameters $K_{Pf}$ and $K_{Df}$ are more sensitive towards the performance index. Hence, for the objective function $F$, the boundary conditions of the six design variables serve as the design constraints and are represented as:

$$K_P^{\min} \leqslant K_P \leqslant K_P^{\max} \tag{15}$$

$$K_I^{\min} \leqslant K_I \leqslant K_I^{\max} \tag{16}$$

$$K_D^{\min} \leqslant K_D \leqslant K_D^{\max} \tag{17}$$

$$n^{\min} \leqslant n \leqslant n^{\max} \tag{18}$$

$$K_{Pf}^{\min} \leqslant K_{Pf} \leqslant K_{Pf}^{\max} \tag{19}$$

$$K_{Df}^{\min} \leqslant K_{Df} \leqslant K_{Df}^{\max} \tag{20}$$

Hence, the problem becomes minimization of (11) using SOS algorithm subject to (15)–(20). Steps for minimization are described as:

Step 1: Define common control parameters like population size $S_{POP}$ and maximum iteration *Iter_MAX*. Initialize random population $X$ for all design variables in search space.
Step 2: Determine best solution, $X_{best}$, by evaluating $F$ defined in (11) for each solution.
Step 3: Modify each solution using (12) and (13) defined in mutualism phase.
Step 4: Evaluate objective function $F$ for each modified solution and select better solutions.
Step 5: Modify each solution using (14) defined in commensalism phase.
Step 6: Evaluate objective function $F$ for each modified solution and select better solutions.
Step 7: Modify each solution according to parasitism phase.
Step 8: Terminate program if the termination criterion is reached otherwise repeat step 2 to step 7.

## 5. Study results and discussion

In present work, a two-area IPS including two non-reheat thermal power plants is considered with presence of DFIG in one area. The nominal parameters of interconnected system are listed in Appendix A [36] and the numerical values of the constants involved in the inertial control scheme of DFIG based generation and the power limit of the non-conventional generator are listed in Appendix B [33]. The ranges of controller-parameters, defined in (15), is listed in Table 2.

The objective function, $F$, formulated in (11) is evaluated using SOS algorithm. In view of testing the superiority of SOS algorithm, thorough assessment is carried out by comparing the obtained results with algorithms like DE, EHO, PSO and TLBO. During all simulations, the common control parameters like population size, $S_{POP}$, and the maximum iteration, *Iter_MAX*, are taken as 20 and 100 for all algorithms, respectively. The algorithm-specific parameters of algorithms used in this work are listed in Table 3.

To have better insights on the performance of proposed controller for improving FRC of wind-integrated IPS, diverse cases of step load perturbations (SLPs) are considered under different wind penetration levels, $W_{PL}$. The considered case studies are categorized as:

**Table 2**
Ranges of controller-parameters.

| Parameters | Range | |
|---|---|---|
| | Minimum | Maximum |
| $K_P$ | 0 | 3 |
| $K_I$ | 0 | 3 |
| $K_D$ | 0 | 3 |
| $n$ | 0 | 500 |
| $K_{Pf}$ | 0 | 3 |
| $K_{Df}$ | 0 | 3 |

**Table 3**
Algorithm-specific parameters and their values.

| Algorithm | Parameter | Value |
|---|---|---|
| ABC | Limit | 50 |
| DE | Mutation factor $M_F$ | 0.8 |
| | Crossover rate $C_R$ | 0.8 |
| EHO | Scale factor $\omega$ | 0.5 |
| | Scale factor $\mu$ | 0.1 |
| PSO | Cognitive parameter $c_1$ | 2 |
| | Social parameter $c_2$ | 2 |
| | Inertia weight $w$ | 0.5 |
| TLBO | NA | NA |
| SOS | NA | NA |

NA – Not applicable.

**Case 1.** 10% $W_{PL}$ without frequency support with 10% SLP, $\Delta P_{d1}$, at $t = 0$ s in area 1.

**Case 2.** 10% $W_{PL}$ without frequency support with 10% SLP, $\Delta P_{d2}$, at $t = 0$ s in area 2.

**Case 3.** 10% $W_{PL}$ with frequency support with 10% SLP, $\Delta P_{d1}$, at $t = 0$ s in area 1.

**Case 4.** 10% $W_{PL}$ with frequency support with 10% SLP, $\Delta P_{d2}$, at $t = 0$ s in area 2.

**Case 5.** 20% $W_{PL}$ without frequency support with 10% SLP, $\Delta P_{d1}$, at $t = 0$ s in area 1.

**Case 6.** 20% $W_{PL}$ without frequency support with 10% SLP, $\Delta P_{d2}$, at $t = 0$ s in area 2.

Under these cases, simulation results in numerical form are presented in various tables comparing the performance of the system with DE, EHO, PSO, TLBO and SOS tuned controllers. To further validate the results listed in tables, TDSs are obtained for the FDs of both areas and the TLPD under all cases.

The simulation results under case 1 are presented in Table 4. The value of defined objective function $F$ and design-objectives $F_1, F_2$, and $F_3$ along with the tuned controller parameters ($K_P, K_I, K_D, n, K_{Pf}$, and $K_{Df}$) obtained with different algorithms (DE, EHO, PSO, TLBO, and SOS) are presented in the table. The table also lists the STs ($\Delta f_1^{st}, \Delta f_2^{st}$, and $\Delta P_{tie}^{st}$) and POs ($\Delta f_1^{po}, \Delta f_2^{po}$, and $\Delta P_{tie}^{po}$) of the FDs of both areas and TLPD. The ITAE of the system is listed in the table too. After a close look at the table, it can be seen that the value of objective function $F$, i.e. **1.4188**, is minimum for the system with SOS-based controller. Additionally, the values of design objectives $F_1$ and $F_2$ obtained for the system with proposed controller are found to be **8.1750** and **0.1381**, respectively which are minimum. Hence, from the Table 4, it can be inferred that the system with SOS tuned controller is better performer in comparison to the system with other controllers. It is obvious from the results that the STs of FDs and TLPD are minimum for the system with proposed controller since the value of design objective $F_1$ is minimum. The TDSs for case 1 are presented in Fig. 4. In Fig. 4 (a), FD of area 1 is shown. The FD for area 2 is shown in Fig. 4 (b). In Fig. 4 (c), the TLPD is depicted. From all the figures, it can be easily observed that the system with SOS-based controller is performing better than others.

The simulation results for case 2 are presented in Table 5. From the table, it can be seen that the value of objective function $F$, i.e. **1.4420** is minimum for the system with proposed controller. The minimum value of design objective $F_1$, i.e. **13.2737**, is obtained for the system with proposed controller. The tuned controller parameters are also listed in the table. Overall analysis of the table affirms the better performance of the system with proposed controller in comparison to others. In Fig. 5, the TDSs for this case are illustrated. The observation of the figures reveals better performance of the system with proposed controller. From the above discussion, it can be concluded that the system with proposed

**Table 4**
Simulation results for Case 1.

| | | DE-*PIDn* | EHO-*PIDn* | PSO-*PIDn* | TLBO-*PIDn* | SOS-*PIDn* |
|---|---|---|---|---|---|---|
| Objective | $F$ | 1.6611 | 1.7001 | 1.7345 | 1.7716 | **1.4188** |
| | $F_1$ | 20.4711 | 16.0370 | 16.3419 | 17.7672 | 8.1750 |
| | $F_2$ | 0.3446 | 0.2226 | 0.2052 | 0.3104 | 0.1381 |
| | $F_3$ | 0.0908 | 0.0885 | 0.1224 | 0.0854 | 0.2222 |
| Controller | $K_P$ | 0.1833 | 0.5500 | 0.6457 | 0.0833 | 0.8707 |
| | $K_I$ | 1.7967 | 2.4056 | 2.3415 | 2.0288 | 2.0585 |
| | $K_D$ | 1.5564 | 1.5412 | 0.6817 | 1.8712 | 0.4095 |
| | $n$ | 414.2287 | 302.5039 | 305.0695 | 310.7500 | 284.77 |
| | $K_{Pf}$ | 1.6705 | 2.1219 | 1.7150 | 1.2656 | 1.1619 |
| | $K_{Df}$ | 0.9628 | 0.8962 | 0.9554 | 0.0264 | 0.8830 |
| Settling | $\Delta f_1^{st}$ | 5.2805 | 4.0109 | 4.0189 | 4.5511 | 2.8552 |
| | $\Delta f_2^{st}$ | 7.7741 | 6.1023 | 6.1308 | 6.5925 | 2.5569 |
| | $\Delta P_{tie}^{st}$ | 7.4165 | 5.9237 | 6.1923 | 6.6236 | 2.7628 |
| ITAE | | 0.3446 | 0.2226 | 0.2052 | 0.3104 | 0.1381 |
| Peak over-shoots (p.u.) | $\Delta f_1^{po}$ | 0.0611 | 0.0612 | 0.0827 | 0.0563 | 0.1252 |
| | $\Delta f_2^{po}$ | 0.0212 | 0.0195 | 0.0288 | 0.0206 | 0.0722 |
| | $\Delta P_{tie}^{po}$ | 0.0086 | 0.0077 | 0.0109 | 0.0084 | 0.0248 |

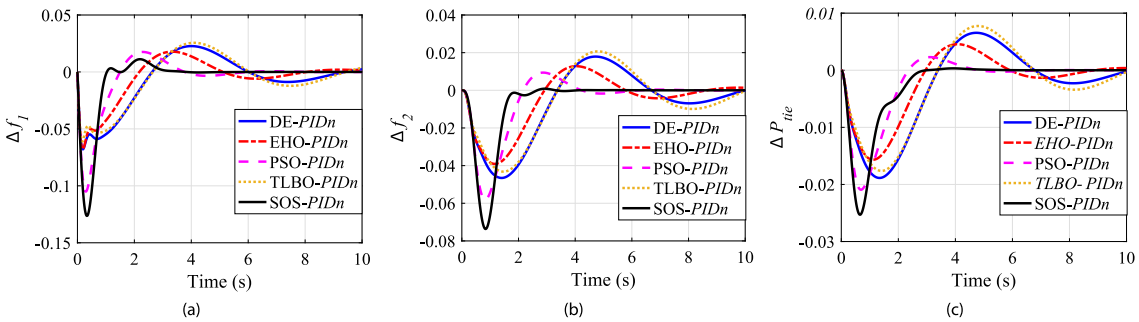


**Fig. 4.** TDSs for Case 1. (a) FD in area 1. (b) FD in area 2. (c) TLPD.

**Table 5**
Simulation results for Case 2.

| | | DE-*PIDn* | EHO-*PIDn* | PSO-*PIDn* | TLBO-*PIDn* | SOS-*PIDn* |
|---|---|---|---|---|---|---|
| Objective | $F$ | 1.5128 | 1.5531 | 1.6153 | 1.4734 | **1.4420** |
| | $F_1$ | 20.8226 | 21.9762 | 20.7383 | 13.6297 | 13.2737 |
| | $F_2$ | 0.9369 | 3.0038 | 0.3383 | 0.2499 | 0.2644 |
| | $F_3$ | 0.0956 | 0.1289 | 0.1226 | 0.2539 | 0.2012 |
| Controller | $K_P$ | 1.5697 | 1.9808 | 1.0984 | 0.7505 | 0.9301 |
| | $K_I$ | 0.9299 | 0.0674 | 2.3075 | 1.9697 | 1.4350 |
| | $K_D$ | 1.6280 | 0.8485 | 0.9662 | 0.2441 | 0.7052 |
| | $n$ | 459.3777 | 295.9935 | 152.7902 | 404.38 | 274.38 |
| | $K_{Pf}$ | 0.8585 | 1.1670 | 1.9639 | 1.1587 | 1.2542 |
| | $K_{Df}$ | 0.6687 | 0.1665 | 2.1552 | 1.2423 | 0.5834 |
| Settling | $\Delta f_1^{st}$ | 9.6658 | 8.3024 | 6.9716 | 4.3830 | 4.7413 |
| | $\Delta f_2^{st}$ | 3.1923 | 4.3929 | 6.7403 | 4.4165 | 4.0647 |
| | $\Delta P_{tie}^{st}$ | 7.9644 | 9.2810 | 7.0265 | 4.8302 | 4.4676 |
| ITAE | | 0.9369 | 3.0038 | 0.3383 | 0.2499 | 0.2644 |
| Peak over-shoots (p.u.) | $\Delta f_1^{po}$ | 0.0186 | 0.0250 | 0.0244 | 0.0903 | 0.0506 |
| | $\Delta f_2^{po}$ | 0.0583 | 0.0810 | 0.0795 | 0.1356 | 0.0753 |
| | $\Delta P_{tie}^{po}$ | 0.0186 | 0.0230 | 0.0187 | 0.0280 | 0.0753 |

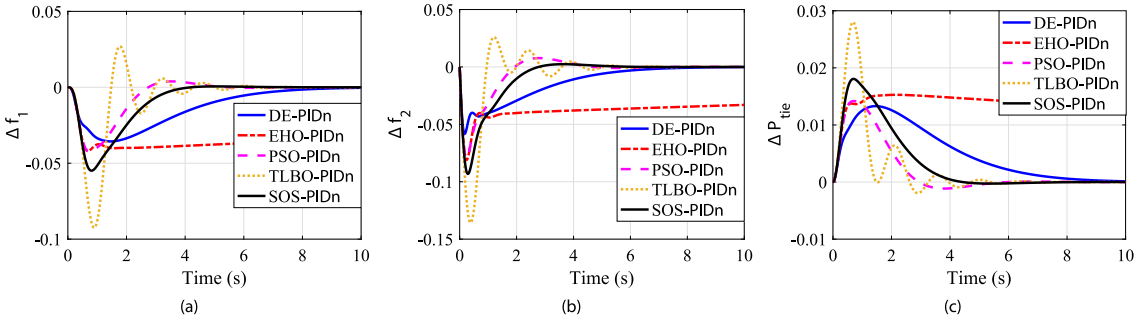


**Fig. 5.** TDSs for Case 2. (a) FD in area 1. (b) FD in area 2. (c) TLPD.

controller is performing better when there is wind penetration without providing frequency support.

Table 6 shows the simulation results of the system under case 3. In this case, the frequency support given by DFIG is considered which improves the FRC of the integrated system. The value of objective function $F$ found to be **1.5077** which is minimum for the system with proposed controller. Additionally, the value of design objective $F_1$, equal to **8.7191**, and design objective $F_2$, equal to **0.1922**, are minimum for the system with proposed controller. The value of tuned controller parameters under this case are listed in the same table. The careful examination of the table affirms the better performance of the proposed controller in terms of considered objectives. The TDSs for case 3 are presented in Fig. 6. In Fig. 6 (a), FD of area 1 is shown. The FD for area 2 is shown in

**Table 6**
Simulation results for Case 3.

| | | DE-*PIDn* | EHO-*PIDn* | PSO-*PIDn* | TLBO-*PIDn* | SOS-*PIDn* |
|---|---|---|---|---|---|---|
| Objective | $F$ | 1.6033 | 1.7118 | 1.7453 | 1.8442 | **1.5077** |
| | $F_1$ | 16.0614 | 19.2495 | 19.4861 | 15.2823 | 8.7191 |
| | $F_2$ | 3.3410 | 0.2606 | 0.2327 | 3.0679 | 0.1922 |
| | $F_3$ | 0.1348 | 0.0857 | 0.0884 | 0.0989 | 0.2567 |
| Controller | $K_P$ | 0.5372 | 0.8538 | 1.4413 | 1.1728 | 0.6019 |
| | $K_I$ | 0.0184 | 2.1696 | 2.3985 | 0.0231 | 1.6859 |
| | $K_D$ | 0.4622 | 1.5323 | 1.3607 | 1.3430 | 0.2937 |
| | $n$ | 241.2474 | 297.7588 | 328.4863 | 345.3562 | 297.50 |
| | $K_{Pf}$ | 1.4972 | 0.5453 | 1.4670 | 1.0174 | 1.4119 |
| | $K_{Df}$ | 1.0991 | 2.2447 | 0.3961 | 0.0810 | 0.9911 |
| Settling | $\Delta f_1^{st}$ | 5.0972 | 4.9074 | 4.8516 | 3.7164 | 2.9870 |
| | $\Delta f_2^{st}$ | 5.5620 | 7.2539 | 7.2826 | 5.7648 | 2.9342 |
| | $\Delta P_{tie}^{st}$ | 5.4023 | 7.0882 | 7.3519 | 5.8011 | 2.7978 |
| ITAE | | 3.3410 | 0.2606 | 0.2327 | 3.0679 | 0.1922 |
| Peak over-shoots (p.u.) | $\Delta f_1^{po}$ | 0.0888 | 0.0591 | 0.0615 | 0.0622 | 0.1385 |
| | $\Delta f_2^{po}$ | 0.0330 | 0.0190 | 0.0197 | 0.0258 | 0.0880 |
| | $\Delta P_{tie}^{po}$ | 0.0130 | 0.0076 | 0.0072 | 0.0110 | 0.0301 |

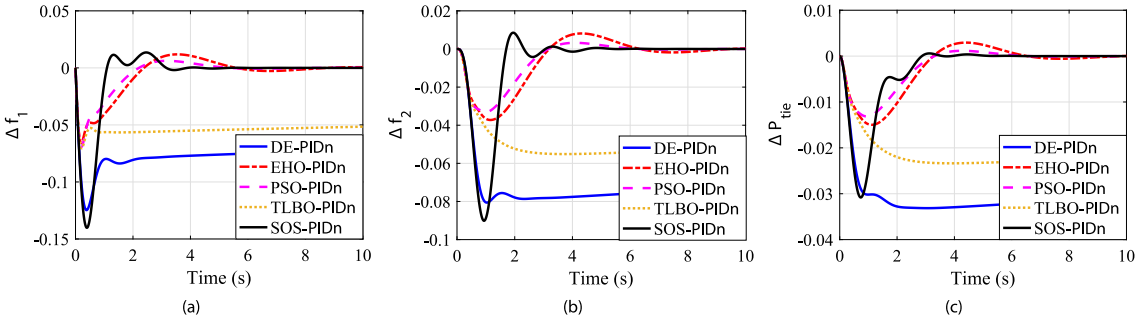


**Fig. 6.** TDSs for Case 3. (a) FD in area 1. (b) FD in area 2. (c) TLPD.

Fig. 6 (b). The Fig. 6 (c) shows TLPD. The observation of the figures reveals that the system with SOS-based controller is performing better than others.

Table 7 lists the obtained results for case 4. In this case, the minimum value of the objective function $F$, equal to **1.3641**, is obtained for the system with the proposed controller. The value of the design objectives $F_1$, equal to **8.3745**, and $F_2$, equal to **0.1540**, are also found to be minimum for the system with proposed controller. The value of tuned controller parameters for this case are listed in the table for different controllers. The TDSs for this case are depicted in Fig. 7. From the figure, it is verified that the STs of FDs and TLPD are less for the system with proposed controller in comparison to others on most occasions. The above discussion suggests superior performance of the SOS-based controller for the system with wind penetration providing frequency support.

In Table 8, the simulation results under case 5 are presented. It can be found from the table that the value of objective function $F$, equal to **1.5632**, is minimum for the system with proposed controller. The value of design objective $F_1$, equal to **10.4433**, is found to be minimum for the system with SOS tuned controller. The tuned controller parameters under this case for different controllers are listed in the same table. In Fig. 8, the TDSs for FDs and TLPD are presented for case 5. The superior performance of the system with SOS-based controller can be easily identified from the figures.

The simulation results for the system under case 6 are shown in Table 9. In this table, it can be observed that the minimum value of

**Table 7**
Simulation results for Case 4.

| | | DE-*PIDn* | EHO-*PIDn* | PSO-*PIDn* | TLBO-*PIDn* | SOS-*PIDn* |
|---|---|---|---|---|---|---|
| Objective | $F$ | 1.5593 | 1.4265 | 1.5842 | 1.6314 | **1.3641** |
| | $F_1$ | 16.2675 | 17.6234 | 19.8680 | 18.9262 | 8.3745 |
| | $F_2$ | 4.3675 | 0.4238 | 1.0433 | 0.4263 | 0.1540 |
| | $F_3$ | 0.1184 | 0.1420 | 0.1387 | 0.1896 | 0.2254 |
| Controller | $K_P$ | 1.0085 | 0.4759 | 1.2167 | 0.4285 | 0.7557 |
| | $K_I$ | 0.0145 | 2.2579 | 0.7932 | 2.1386 | 1.8024 |
| | $K_D$ | 1.9278 | 0.7934 | 0.7809 | 0.3897 | 0.3627 |
| | $n$ | 112.9872 | 406.2541 | 144.2880 | 478.7818 | 352.82 |
| | $K_{Pf}$ | 1.6559 | 0.3800 | 2.0364 | 1.2466 | 0.8641 |
| | $K_{Df}$ | 1.4805 | 0.7800 | 0.9091 | 0.8373 | 1.8470 |
| Settling | $\Delta f_1^{st}$ | 2.5346 | 6.1270 | 9.5407 | 6.5608 | 2.7796 |
| | $\Delta f_2^{st}$ | 6.7021 | 5.9453 | 2.2731 | 5.8712 | 2.8693 |
| | $\Delta P_{tie}^{st}$ | 7.0308 | 5.5511 | 8.0541 | 6.4943 | 2.7255 |
| ITAE | | 4.3675 | 0.4238 | 1.0433 | 0.4263 | 0.1540 |
| Peak over-shoots (p.u.) | $\Delta f_1^{po}$ | 0.0252 | 0.0273 | 0.0270 | 0.0349 | 0.0780 |
| | $\Delta f_2^{po}$ | 0.0558 | 0.0902 | 0.0881 | 0.1235 | 0.1220 |
| | $\Delta P_{tie}^{po}$ | 0.0374 | 0.0245 | 0.0236 | 0.0312 | 0.0253 |

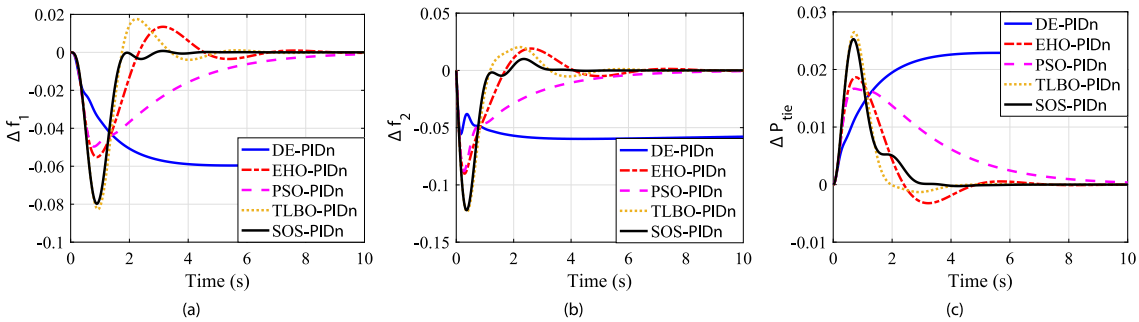


**Fig. 7.** TDSs for Case 4. (a) FD in area 1. (b) FD in area 2. (c) TLPD.

**Table 8**
Simulation results for Case 5.

| | | DE-*PIDn* | EHO-*PIDn* | PSO-*PIDn* | TLBO-*PIDn* | SOS-*PIDn* |
|---|---|---|---|---|---|---|
| Objective | $F$ | 1.8127 | 1.6876 | 1.6495 | 1.6714 | **1.5632** |
| | $F_1$ | 15.1156 | 11.7334 | 12.5574 | 11.6873 | 10.4433 |
| | $F_2$ | 0.4369 | 0.2581 | 0.2791 | 0.1947 | 0.2944 |
| | $F_3$ | 0.3005 | 0.1330 | 0.2443 | 0.1429 | 0.3072 |
| Controller | $K_P$ | 0.1804 | 1.6486 | 0.7639 | 1.8798 | 0.5396 |
| | $K_I$ | 1.4758 | 1.7649 | 1.2747 | 1.9522 | 1.5000 |
| | $K_D$ | 0.3457 | 1.2490 | 0.4530 | 1.0403 | 0.2204 |
| | $n$ | 444.9136 | 237.8460 | 197.3753 | 394.0227 | 353.28 |
| | $K_{Pf}$ | 1.4950 | 0.4884 | 0.6662 | 1.4362 | 0.5358 |
| | $K_{Df}$ | 1.7874 | 0.0366 | 1.1274 | 0.7128 | 0.8218 |
| Settling | $\Delta f_1^{st}$ | 5.2661 | 2.8726 | 4.0842 | 2.6086 | 2.1300 |
| | $\Delta f_2^{st}$ | 5.3037 | 4.3526 | 4.1000 | 4.4617 | 4.0487 |
| | $\Delta P_{tie}^{st}$ | 4.5458 | 4.5081 | 4.3732 | 4.6170 | 4.2645 |
| ITAE | | 0.4369 | 0.2581 | 0.2791 | 0.2374 | 0.2944 |
| Peak over-shoots (p.u.) | $\Delta f_1^{po}$ | 0.1608 | 0.0829 | 0.1374 | 0.0989 | 0.1678 |
| | $\Delta f_2^{po}$ | 0.1030 | 0.0358 | 0.0790 | 0.0557 | 0.1038 |
| | $\Delta P_{tie}^{po}$ | 0.0366 | 0.0143 | 0.0279 | 0.0222 | 0.0356 |

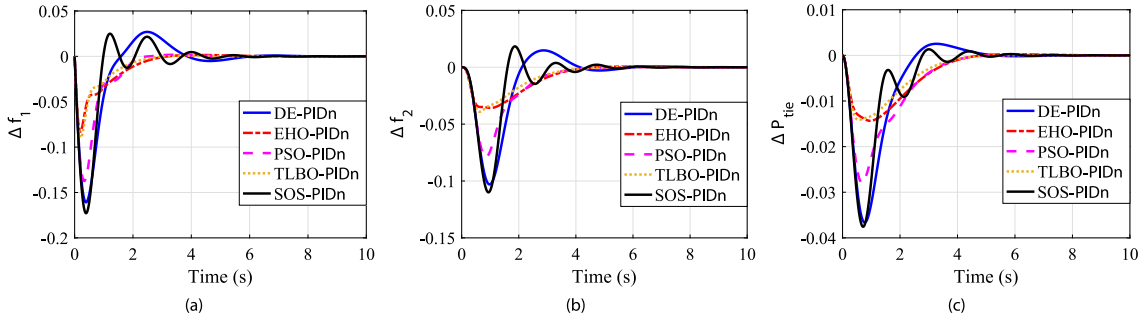


**Fig. 8.** TDSs for Case 5. (a) FD in area 1. (b) FD in area 2. (c) TLPD.

**Table 9**
Simulation results for Case 6.

| | | DE-*PIDn* | EHO-*PIDn* | PSO-*PIDn* | TLBO-*PIDn* | SOS-*PIDn* |
|---|---|---|---|---|---|---|
| Objective | $F$ | 1.6338 | 1.7021 | 1.6565 | 1.6439 | **1.3802** |
| | $F_1$ | 13.9670 | 15.4296 | 14.5325 | 14.9235 | 13.5221 |
| | $F_2$ | 0.5446 | 0.5414 | 0.5553 | 0.6060 | 0.3198 |
| | $F_3$ | 0.1828 | 0.2670 | 0.2357 | 0.2699 | 0.2210 |
| Controller | $K_P$ | 0.5766 | 0.4628 | 0.4292 | 0.2623 | 0.3655 |
| | $K_I$ | 0.9151 | 0.8521 | 0.8399 | 0.7556 | 1.4932 |
| | $K_D$ | 0.6902 | 0.2855 | 0.4148 | 0.2517 | 0.4738 |
| | $n$ | 437.0334 | 285.50 | 125.64 | 294.11 | 482.93 |
| | $K_{Pf}$ | 0.3353 | 1.6961 | 1.6955 | 1.3495 | 0.0001 |
| | $K_{Df}$ | 1.5683 | 1.8561 | 0.8554 | 1.3259 | 1.3285 |
| Settling | $\Delta f_1^{st}$ | 4.9459 | 5.8018 | 5.6769 | 5.4373 | 4.5434 |
| | $\Delta f_2^{st}$ | 3.8020 | 4.6764 | 4.1287 | 4.0758 | 3.8443 |
| | $\Delta P_{tie}^{st}$ | 5.2192 | 4.9513 | 4.7269 | 5.4104 | 5.1343 |
| ITAE | | 0.5446 | 0.5414 | 0.5553 | 0.6060 | 0.3198 |
| Peak over-shoots (p.u.) | $\Delta f_1^{po}$ | 0.0660 | 0.0988 | 0.0857 | 0.0746 | 0.0798 |
| | $\Delta f_2^{po}$ | 0.0968 | 0.1381 | 0.1235 | 0.1633 | 0.1166 |
| | $\Delta P_{tie}^{po}$ | 0.0200 | 0.0300 | 0.0264 | 0.0320 | 0.0245 |

objective function $F$, equal to **1.3802**, is obtained for the system with proposed controller. The minimum values of design objective $F_1$, equal to **13.5221**, and design objective $F_2$, equal to **0.3198**, are also obtained for the system with proposed controller. The same table lists the tuned controller parameters under this case. The TDSs for this case are illustrated in Fig. 9. A closer observation of the figure affirms that the FDs of the two areas and the TLPD are settling down quickly for the system with SOS based controller. It can be inferred from the above discussion that the performance of proposed controller is better for the system even with large penetration of wind generation.

As discussed earlier that it is a vital requirement of the system to settle down the FDs and TLPD as soon as possible after an occurrence of the disturbance in an IPS in order to maintain stability.

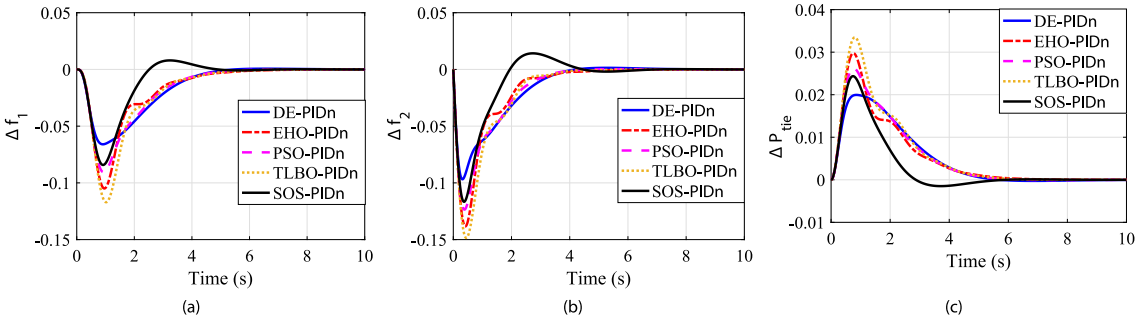


**Fig. 9.** TDSs for Case 6. (a) FD in area 1. (b) FD in area 2. (c) TLPD.

Owing to the above cited reason, in this present work, the objective function $F_1$ i.e. the sum of the STs of FDs of both areas and the TLPD is given much importance compared to other objective functions $F_2$ and $F_3$. And, the same is represented in combined objective function $F$ defined in (11). From the simulation results presented in Tables 4–9, it is observed that the minimum value of the objective function $F$ is always obtained for the system with SOS-based controller which is an indicator of better performance of the system with SOS-based controller in comparison to others. The TDSs are presented for all cases which further support the claim of better performance of the system with proposed controller.

## 6. Conclusion

In this work, SOS algorithm based coordinated tuning of controller-parameters for improving FRC of a wind-integrated IPS is presented. A two-area thermal power plant is considered with one area integrated with DFIG based WPG. The integration of DFIG based WPG is primarily for improving FR of whole system. The inertial control scheme for DFIG based WPG is adopted for regulating frequency of the system. To test the efficacy of system with proposed controller, the system is subjected to diverse sets of disturbances under different wind penetration levels with or without frequency support. The superior performance of the system with proposed controller is established by comparing its results with the results obtained for the system with four different controllers. Further, the effective performance of the system with proposed controller is determined by the presented TDSs for FDs and TLPD for considered cases. The simulation results and TDSs also prove the superiority of SOS-based controller. The future work lies in the exploration of system performance with proposed controller after including non-linearity and governor dead-band into the thermal interconnected system.

## Appendix A. Nominal parameters of two-area IPS.

$H_1 = H_2 = 5, R_1 = R_2 = 2.4$ Hz/p.u. MW, $B_1 = B_2 = 0.425$, $T_{G1} = T_{G2} = 0.08$ s, $T_{T1} = T_{T2} = 0.3$ s, $K_{PS1} = K_{PS2} = 120$ Hz/p.u. MW, $T_{PS1} = T_{PS2} = 20$ s, $f_1 = f_2 = 60$ Hz, $T_{12} = 0.0867$ s, $a_{12} = -1$. Total capacity of areas is $P_{g1} = P_{g2} = 2000$ MW.

## Appendix B. Nominal parameters of DFIG.

For 20% wind penetration, the values of $R$ and $H$ change as given in Table 1. The values of other parameters (constants) are $B_1 = B_2 = 0.3417, T_{PS1} = T_{PS2} = 18.8415$ s, $H = 3.5$ s, $T_W = 6$ s, $T_R = 0.2$ s, $T_G = 0.2$ s, $K_{Wi} = 0.15$ s, $K_{Wp} = 1.5, P_G^{\min} = 0$ p.u., $P_G^{\max} = 1.2$ p.u., $\omega_{ref} = 1$ p.u.

## References


[1] O.I. Elgerd, Electric energy systems theory: an introduction.
[2] P. Kundur, N.J. Balu, M.G. Lauby, Power System Stability and Control, vol. 7, McGraw-hill, New York, 1994.
[3] B.H. Chowdhury, H.T. Ma, Frequency regulation with wind power plants, Power and Energy Society General Meeting-Conversion and Delivery of Electrical Energy in the 21st Century, IEEE, 2008, pp. 1–5.
[4] E. Eltra, Wind turbines connected to grids with voltages above 100 kv, Regulation document TF 3 (5).
[5] F. Van Hulle, Large Scale Integration of Wind Energy in the European Power Supply: Analysis, Issues and Recommendations Executive Summary, European Wind Energy Association, 2005.
[6] N.R. Ullah, T. Thiringer, D. Karlsson, Temporary primary frequency control support by variable speed wind turbines–potential and applications, IEEE Trans. Power Syst. 23 (2) (2008) 601–612.
[7] J. Ekanayake, N. Jenkins, Comparison of the response of doubly fed and fixed-speed induction generator wind turbines to changes in network frequency, IEEE Trans. Energy Conversion 19 (4) (2004) 800–802.
[8] A. Mullane, M. O'Malley, The inertial response of induction-machine-based wind turbines, IEEE Trans. Power Syst. 20 (3) (2005) 1496–1503.
[9] J. Morren, J. Pierik, S.W. De Haan, Inertial response of variable speed wind turbines, Electric Power Syst. Res. 76 (11) (2006) 980–987.
[10] G. Lalor, A. Mullane, M. O'Malley, Frequency control and wind turbine technologies, IEEE Trans. Power Syst. 20 (4) (2005) 1905–1913.
[11] O. Anaya-Lara, F. Hughes, N. Jenkins, G. Strbac, Contribution of dfig-based wind farms to power system short-term frequency regulation, IEE Proc.-Gener., Transm. Distrib. 153 (2) (2006) 164–170.
[12] J. Morren, S.W. De Haan, W.L. Kling, J. Ferreira, Wind turbines emulating inertia and supporting primary frequency control, IEEE Trans. Power Syst. 21 (1) (2006) 433–434.
[13] J.M. Mauricio, A. Marano, A. Gómez-Expósito, J.L.M. Ramos, Frequency regulation contribution through variable-speed wind energy conversion systems, IEEE Trans. Power Syst. 24 (1) (2009) 173–180.
[14] P. Bhatt, R. Roy, S. Ghoshal, Dynamic participation of doubly fed induction generator in automatic generation control, Renewable Energy 36 (4) (2011) 1203–1213.
[15] R. Ahmadi, A. Sheikholeslami, A. Nabavi Niaki, A. Ranjbar, Dynamic participation of doubly fed induction generators in multi–control area load frequency control, Int. Trans. Electr. Energy Syst. 25 (7) (2015) 1130–1147.
[16] N. Rathore, D. Chauhan, V. Singh, Luus-jaakola optimization procedure for pid controller tuning in reverse osmosis system, in: International Conference on Electrical, Electronics, and Robotics (IRAJ-IACEER, 2015.
[17] S. Gupta, V. Singh, S. Singh, T. Prakash, N. Rathore, Elephant herding optimization based pid controller tuning, Int. J. Adv. Technol. Eng. Exploration 3 (24) (2016) 194.
[18] S.P. Singh, T. Prakash, V. Singh, M.G. Babu, Analytic hierarchy process based automatic generation control of multi-area interconnected power system using jaya algorithm, Eng. Appl. Artif. Intell. 60 (2017) 35–44.
[19] S.P. Ghoshal, Optimizations of pid gains by particle swarm optimizations in fuzzy based automatic generation control, Electric Power Syst. Res. 72 (3) (2004) 203–212.
[20] H. Gozde, M.C. Taplamacioglu, Automatic generation control application with craziness based particle swarm optimization in a thermal power system, Int. J. Electr. Power Energy Syst. 33 (1) (2011) 8–16.
[21] S. Panda, N.K. Yegireddy, Automatic generation control of multi-area power system using multi-objective non-dominated sorting genetic algorithm-ii, Int. J. Electr. Power Energy Syst. 53 (2013) 54–63.
[22] U.K. Rout, R.K. Sahu, S. Panda, Design and analysis of differential evolution algorithm based automatic generation control for interconnected power system, Ain Shams Eng. J. 4 (3) (2013) 409–421.
[23] H. Gozde, M.C. Taplamacioglu, I. Kocaarslan, Comparative performance analysis of artificial bee colony algorithm in automatic generation control for interconnected reheat thermal power system, Int. J. Electr. Power Energy Syst. 42 (1) (2012) 167–178.

[24] B.K. Sahu, S. Pati, P.K. Mohanty, S. Panda, Teaching–learning based optimization algorithm based fuzzy-pid controller for automatic generation control of multi-area power system, Appl. Soft Comput. 27 (2015) 240–249.
[25] K. Naidu, H. Mokhlis, A. Bakar, V. Terzija, H. Illias, Application of firefly algorithm with online wavelet filter in automatic generation control of an interconnected reheat thermal power system, Int. J. Electr. Power Energy Syst. 63 (2014) 401–413.
[26] L. Shi, C. Wang, L. Yao, Y. Ni, M. Bazargan, Optimal power flow solution incorporating wind power, IEEE Syst. J. 6 (2) (2012) 233–241.
[27] A. Panda, M. Tripathy, Optimal power flow solution of wind integrated power system using modified bacteria foraging algorithm, Int. J. Electr. Power Energy Syst. 54 (2014) 306–314.
[28] A. Panda, M. Tripathy, Security constrained optimal power flow solution of wind-thermal generation system using modified bacteria foraging algorithm, Energy 93 (2015) 816–827.
[29] A. Panda, M. Tripathy, A. Barisal, T. Prakash, A modified bacteria foraging based optimal power flow framework for hydro-thermal-wind generation system in the presence of statcom, Energy 124 (2017) 720–740.
[30] P. Bhatt, S. Ghoshal, R. Roy, Coordinated control of tcps and smes for frequency regulation of interconnected restructured power systems with dynamic participation from dfig based wind farm, Renewable Energy 40 (1) (2012) 40–50.
[31] S.K. Pandey, S.R. Mohanty, N. Kishor, J.P. Catalào, Frequency regulation in hybrid power systems using particle swarm optimization and linear matrix inequalities based robust controller design, Int. J. Electr. Power Energy Syst. 63 (2014) 887–900.
[32] Y.K. Bhateshvar, H.D. Mathur, H. Siguerdidjane, S. Bhanot, Frequency stabilization for multi-area thermal–hydro power system using genetic algorithm-optimized fuzzy logic controller in deregulated environment, Electric Power Components Syst. 43 (2) (2015) 146–156.
[33] S. Chaine, M. Tripathy, S. Satpathy, NSGA-II based optimal control scheme of wind thermal power system for improvement of frequency regulation characteristics, Ain Shams Eng. J. 6 (3) (2015) 851–863.
[34] S. Chaine, M. Tripathy, D. Jain, Non dominated cuckoo search algorithm optimized controllers to improve the frequency regulation characteristics of wind thermal power system, Engineering Science and Technology, an International Journal.
[35] K. Deb, Multi-objective genetic algorithms: Problem difficulties and construction of test problems, Evolutionary Comput. 7 (3) (1999) 205–230.
[36] E. Ali, S. Abd-Elazim, Bacteria foraging optimization algorithm based load frequency controller for interconnected power system, Int. J. Electr. Power Energy Syst. 33 (3) (2011) 633–638.
[37] X. Yingcheng, T. Nengling, Review of contribution to frequency control through variable speed wind turbine, Renewable Energy 36 (6) (2011) 1671–1677.
[38] R.G. de Almeida, E.D. Castronuovo, J.P. Lopes, Optimum generation control in wind parks when carrying out system operator requests, IEEE Trans. Power Syst. 21 (2) (2006) 718–725.
[39] F.M. Hughes, O. Anaya-Lara, N. Jenkins, G. Strbac, Control of dfig-based wind generation for power network support, IEEE Trans. Power Syst. 20 (4) (2005) 1958–1966.
[40] T.L. Saaty, Fundamentals of decision making and priority theory with the analytic hierarchy process, vol. vi, Universitas Pittsburgh. USA.
[41] S. Singh, V. Singh, V. Singh, Analytic hierarchy process based approximation of high-order continuous systems using tlbo algorithm, Int. J. Dyn. Control (2018) 1–8.
[42] M.-Y. Cheng, D. Prayogo, Symbiotic organisms search: a new metaheuristic optimization algorithm, Comput. Struct. 139 (2014) 98–112.